Proceedings of the 5th WSEAS Int. Conf. on Signal Processing, Robotics and Automation, Madrid, Spain, February 15-17, 2006 (pp33-39)

Wavelet analysis applied to the study of digitalized bullet striatures for the firearm identification: first evidences

NIOLA VINCENZO[1], BUCCELLI CLAUDIO[2], GERVASIO LUCA[2], PILLERI MICHELE[2], POLICINO FABIO[2] , QUAREMBA GIUSEPPE[2]

[1]Department of Mechanical Engineering for Energetics
University of Naples "Federico II"
Via Claudio 21, 80125, Napoli
ITALY
http://niola.dime.unina.it

[2]Dipartimento di Medicina Pubblica e della Sicurezza Sociale
University of Naples "Federico II"
Via S. Pansini 5, 80131, Napoli
ITALY

Abstract: - The firearm identification through fired bullets involves the analysis of signs by studying their features. The aim of this paper is to propose a method based on the comparison of multilevel wavelet analysis applied to the digitalized images of the bullet surface.

Key-Words: - forensic ballistics, gun crime, gun investigation, image analysis, firearm identification, wavelet analysis, Radon Transform, Hough Transform

1 Introduction

The bullet, after the passage in a firearm barrel, shows perennial and "characteristic" signs on its surface (macro-striatures, micro-prints and micro-striatures) whose analyses in forensic ballistics are fundamental for the firearm identification.
Macro-striatures are employed to define the firearm "class identification" (*i.e.*, mark and model), while micro-prints and micro-striatures are particular "signs" distinctive of each arm, due to its production and utilization.
Generally, the bullet surface analysis is performed visually through the direct observation of an expert operator and, therefore, it is affected by his subjectivity. In order to structure the diagnosis, in terms of exclusion, compatibility or certainty of firearm identification, Nichols [1][2] has emphasized the problem of researching methods based exclusively on objective evidences [3][4].
Biasotti and Murdock individuated three different methodological approaches (*i.e.*, empirical studies, mechanical and mathematical models) for the identification of the firearm [5][6]. They expressed the necessity that every method was based on objective quantitative and/or qualitative evidences provided by the analysis of the striatures showed by the bullet surface. The empirical studies performed by Nichols (*op. cit.*) were based on the *experience* of a single operator, therefore, they are relatively reliable. In order to state the relationship between two different signs, many mechanical models have been developed. On the other side several mathematical models are finalized to obtain more objective results.
Furthermore, may authors criticized the validity of c*onsecutive matching striation criteria* employed for the measurement of striatures based on their overlapping level [7].
Our previous study, starting from the consideration that the microscopical image analysis of striatures put limits to their interpretation, pointed-out the *coarse* content of information showed by digitalized images because of their low resolution [8]. Nowadays, these limits have been overcome. In fact, recent technological improvements allow to capture and to archive digitalized high resolution images.
Furthermore, it is possible to perform comparative mathematical analyses on them in order to obtain a more quantitatively and qualitatively information as well as more repeatable and reliable results.
At beginning of 90s the Forensic Technology Inc. developed and patented an automatic ballistic bullets and cartridge cases imaging and analysis

system named Integrated Ballistic Identification System (I.B.I.S.) whose results have been illustrated by the Boston Police Department's Ballistics Unit [9].
Our experience focused on processing the microprints and micro-striatures showed by digitalized images of bullet. It allows the development of a comparative method based on multilevel wavelet transform analysis and a pre-filtered process performed by means of the Radon Transform.

2 Material and methods

2.1 Digital equipment and general remarks

The method is based on the following operative phases:

1. repertory and treatment of bullet;
2. surface acquisition of bullet image;
3. image pre-processing (through Radon Transform);
4. Multilevel analysis (through Wavelet Transform).

Three bullets, of calibre 9x21 mm, were examined. These bullets were fired by two guns of the same model: Beretta 98F (indicated in the following as A and B). The bullets were symbolically indicated as 1A, 2A and 1B.
The digitalized images of the bullet surface were acquired, in accordance with a predefined protocol, by a digital reflex camera (Canon Eos 350D) equipped with a CMOS sensor of 8.0 mega-pixel. The camera was fixed to Leitz comparator microscope.
The images, enlarged with 1:4 ratio, were directly sent to CMOS sensor.
The final image enlargement was 32x. It was obtained by a comparison microscope, equipped with 8x zoom lens.
Notice that this is called a macroscope and not a microscope. Microscopes typically use objectives that are 100x and above. Magnifications typically used in firearms identification are 5x, 10x, 20x, 30x, and 40x. It is not unusual however to see this lower powered scope referred to a microscope.
An incandescence ring light, integrated in the ocular and perpendicular to the capture plan, was used as lighting source.
The firearms employed in this work generate, on bullet surface, six macro-striatures (identified by one letter from *a* to *f)*. These six images were obtained by rotating the bullet six times of an angle of 60° with respect to its longitudinal axis. On each macro-striature, a vertical Region of Interest (ROI) (1mm large and located at 3-4 mm from the ogive) has been manually selected. All the ROIs have been pre-processed through algorithms illustrated in the next paragraph.
Successively, to each pre-processed ROI was applied the Multiresolution Wavelet Analysis. It provides the detail decomposition coefficients according to the wavelet function selected.
Consequently, each ROI was decomposed into 13 wavelet detail levels and the analysis was performed by comparing the *rescaled* wavelet detail coefficients.
Moreover, several indexes and parameters have been calculated such as multiple autoregressive and autocorrelation coefficient, energetic contents (*i.e.*, entropy), which will be employed further for deeper examination.
In particular, the diagnosis, in terms of exclusion, compatibility or certainty of the firearm identification, was performed by means of the visual observation of the *best matching* between the two series of the 4^{th} decomposition wavelet level evaluated starting from each of 6 micro-striatures.
For the data computing it has been used the software MATLAB 5.3, The Math Works, Inc, Natick, Mass.

2.2 Mathematical background

2.2.1 The Hough and Radon Transforms

In recent years the Hough transform (*HT*) and the related Radon transform (*RT*) have received much attention. The Hough technique is particularly useful for computing a global description of a feature (where the number of solution classes need not be known *a priori*), given (possibly noisy) local measurements. The main idea behind the Hough technique for line detection is that each input measurement (*e.g.*, coordinate point) indicates its contribution to a globally consistent solution (*e.g.*, the physical line which gave rise to that image point). There is some confusion in the literature regarding how the *HT* and the *RT* are related. It is a problem of definition. A common opinion, which here will be used for defining the *HT*, is that the *HT* maps the individual pixel from the image domain into a shape in the parameter domain [10]. The *RT* transforms a shape in the image domain into a single pixel in the parameter domain. As consequence the *HT* can be derived from the *RT* [11].
The two transforms are able to transform two dimensional images with lines into a domain of

possible line parameters, where each line in the image will give a peak positioned at the corresponding line parameters.
In fact, any point source is modelled as a product of two Dirac delta functions. Initially the point is placed in the origin of the coordinate system [12]

$$g(x,y) = \delta(x)\,\delta(y) \Rightarrow \qquad (1)$$

$$\tilde{g}(p,\tau) = \int_{-\infty}^{\infty} \delta(x)\,\delta(px+\tau)dx = \delta(\tau) \qquad (2)$$

where $g(x,y)$ is a two-dimensional function, $\tilde{g}(p,\tau)$ is the RT, p and τ are the two line parameters indicating slope and line offset respectively.
For each point in the image $g(x^*,y^*)$, by invoking the RT property of shifted function, the point source could be placed at any given position and consequently

$$g(x,y) = \int_{-\infty}^{\infty}\int_{-\infty}^{\infty} g(x^*,y^*)\,\delta(x-x^*)\,\delta(y-y^*)dx^*dy^* \Rightarrow$$

$$\tilde{g}(p,\tau) = \int_{-\infty}^{\infty}\int_{-\infty}^{\infty}\int_{-\infty}^{\infty} g(x^*,y^*)\,\delta(x-x^*)\,\delta(\tau+px-y^*)dx^*dy^*dx$$

$$= \int_{-\infty}^{\infty}\int_{-\infty}^{\infty} g(x^*,y^*)\,\delta(y^*-\tau-px^*)dx^*dy^*. \quad (3)$$

The eq.s (3) express the meaning of HT: for each point in the image $g(x^*,y^*)$, a line in the transformed plane, *i.e.*, the parameter domain, could be drawn. The line is found by setting the argument of the last delta function to zero

$$\tau = y^* - px^* \qquad (4).$$

The value $\tilde{g}(p,\tau)$ is function in two-dimensional (p,τ)-space (*i.e.*, Radon space or parameter domain).
If a certain line is modelled with a delta function, the function has non-zero values only if (x,y) lies on the line with certain fixed parameters (p^*,τ^*)

$$g(x,y) = \delta(y-p^*x-\tau^*). \quad (5)$$

Then the RT is given by

$$\tilde{g}(p,\tau) = \int_{-\infty}^{\infty}\int_{-\infty}^{\infty} \delta(y-p^*x-\tau^*)\,\delta(y-px-\tau)dxdy \quad (6)$$

$$= \int_{-\infty}^{\infty} \delta((p-p^*)x+\tau-\tau^*)dx \qquad (7)$$

$$= \begin{cases} \dfrac{1}{|p-p^*|} & for \quad p \neq p^* \\ 0 & for \quad p = p^* \quad and \quad \tau \neq \tau^* \\ \displaystyle\int_{-\infty}^{\infty} \delta(0)dx & for \quad p = p^* \quad and \quad \tau = \tau^* \end{cases}. \quad (8)$$

Note that for $p = p^*$ and $\tau = \tau^*$, the result is written as an infinite function integrated over an infinite interval, hence the result is infinite in that point. If, for now, the finite terms are neglected, the result is that the RT of a line produces a peak (with infinite value) in the parameter domain, and the position of the peak matches the line parameters.
Assuming that the objective is the identification of line parameters p,τ then the sampling distances Δp and $\Delta\tau$ can be derived as follows

$$\Delta\gamma = \left|\frac{\partial\gamma}{\partial\tau}\right|\Delta\tau = \frac{\pi}{\Delta y}\Delta\tau \le \pi \Rightarrow \Delta\tau \le \Delta y \qquad (9)$$

$$\Delta\gamma = \left|\frac{\partial\lambda}{\partial p}\right|\Delta p = \frac{\pi}{\Delta y}|x_m|\Delta p \le \pi \Rightarrow \Delta p \le \frac{\Delta y}{\max|x_m|}. \quad (10)$$

The (9) and (10) can be wrote if the absolute slope $|p|$ is limited. In that case the RT is determined by the function $\sin(\gamma)/\gamma$.
The eq.(10), in particular, shows that the sampling distance Δp depends on $\max|x_m|$. It must be small if $\max|x_m|$ is large. Consequently, in a digital image the parameter domain must be sampled sufficiently dense in order to avoid aliasing problems and the discrete approximations to the RT does not cause aliasing problems.
Another problem arises when images include one or more lines with high slope (nearly vertical lines).
It can be demonstrated that only lines with parameters that lie within the limits of the parameter domain can be identified. In that case, in order to reduce the computational work, it should

be used to limit the discrete parameter domain. It is a general property of the discrete *RT*.
From the following relation

$$g(x,y) = A\delta(x - x^*) \Rightarrow \tilde{g}(p,\tau) = A\int_{-\infty}^{\infty} \delta(x - x^*)dx = A \quad (11)$$

since the *RT* does not depend on the position of the line x^*, another problem, arising from functions with vertical lines, is that this information is not maintained in the parameter domain, hence the position of vertical lines cannot be detected using slant stacking. A way to overcome the described problems is to compute two parameter domains. The first $\tilde{g}(p,\tau)$ is restricted to $-p_{\lim} < p \le p_{\lim}$ and the other $\tilde{g}(\tau,\eta)$ is used to manage the remaining line orientations

$$\tilde{g}(p,\tau) = \int_{-\infty}^{\infty} g(x, px + \tau)dx \qquad (12)$$

and

$$\tilde{g}(\tau,\eta) = \int_{-\infty}^{\infty} g(\tau y + \eta, y)dy\,. \qquad (13)$$

The two ways of describing lines are related

$$y = px + \tau \Rightarrow x = ry + \eta \quad \text{where} \begin{cases} \tau = \dfrac{1}{p} \\ \eta = -\dfrac{\tau}{p} \end{cases}. \quad (14)$$

Thus if $-p_{\lim} < p \le p_{\lim}$ then the other slope parameter should be bounded by $-\frac{1}{p_{\lim}} \le p \le \frac{1}{p_{\lim}}$.

A reasonable value of the limiting slope is

$$p_{\lim} = \frac{\Delta y}{\Delta x}\,. \qquad (15)$$

2.2.2 Overview on Wavelet methodology

Let $X_1, X_2, \ldots, X_N$ be independent identically distributed random variables whose density is unknown. Recall that a wavelet estimator of f may be given by (e.g., [13][14])

$$\hat{f} = \sum_k \hat{a}_{j_0 k}\phi_{j_0 k}(x) + \sum_{j=j_0}^{j_1}\sum_k \hat{b}_{jk}\psi_{jk}(x), \qquad (16)$$

where

$$\psi_{jk}(x) = 2^{j/2}\psi(2^j x - k),$$

$$\phi_{jk}(x) = 2^{j/2}\phi\left(2^j x - k\right), \quad k \in \mathrm{Z},$$

$$\hat{a}_{j_0 k} = \frac{1}{n}\sum_{i=1}^{n}\varphi_{j_0 k}(X_i) \text{ and } \hat{b}_{jk} = \frac{1}{n}\sum_{i=1}^{n}\psi_{jk}(X_i).$$

Moreover, ψ(x) is a function (mother wavelet) whose first h ($h \in \mathbf{N}$) moments are zero. φ is a function (father wavelet) orthonormal to ψ(x), according to the L^2 norm [15][16]. It is easy to show that if ψ(x) is a mother wavelet, then also ψ_{ik}(x) is a mother wavelet. Moreover, in this case, the systems of functions $\{\{\varphi_{j_0 k}\}, \{\psi_{jk}\}, k \in \mathbf{Z}, j=0, 1,2,\ldots\}$ is an orthonormal system in $L^2(\mathbf{R})$ [17]. The estimator (16) is based on Parseval Theorem. According to this result, any $h \in L^2(\mathbf{R})$ can be represented as a convergent series [18][19]

$$h(x) = \sum_k a_{j_0 k}\varphi_{j_0 k}(x) + \sum_{j=j_0}^{j_1}\sum_k b_{jk}\psi_{jk}(x), \quad (17)$$

where

$$a_{j_0 k} = \int_{-\infty}^{+\infty} h(x)\cdot\frac{1}{\sqrt{2^{j_0}}}\psi\left(\frac{x-k}{2^{j_0}}\right)dx$$

and

$$b_{jk} = \int_{-\infty}^{+\infty} h(x)\cdot\frac{1}{\sqrt{2^{j}}}\varphi\left(\frac{x-k}{2^{j}}\right)dx\,.$$

2.2.3 Detection of lines convolved with a Wavelet

Consider the model

$$g(x,y) = \psi(y - p^* x - \tau^*) \qquad (18)$$

hence the line has certain parameters (p^*, τ^*). If we compare eq. (18) with eq.(5) it can be noted that wavelet $\psi(\circ)$ has been convolved in the *y*-direction. The wavelet could also have been convolved perpendicularly to the line. In this case the corresponding *RT* is given by

$$\tilde{g}(p,\tau)=\begin{cases}\int_{-\infty}^{\infty}\psi(\tau-\tau^{*})dx & for \quad p=p^{*}\\ \dfrac{1}{\left|p-p^{*}\right|}\int_{-\infty}^{\infty}\psi(\tilde{x})d\tilde{x} & for \quad p\neq p^{*}\end{cases}. \qquad (19)$$

The eq. (19) shows that an angular dependent scaling parameter could be included in the wavelet. In order to have a peak in the parameter domain at the correct parameters, the wavelet should have a global maximum when the argument is zero, *i.e.*, corresponding to the position of the line [20]

$$\psi(0)>\psi(x) \quad \forall x\neq 0\,. \qquad (20)$$

3 Results

An example of ROI of two bullets and relative RT is showed in the following figures (Figg. 1, 2).

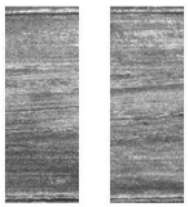

Fig.1 ROI of two bullets

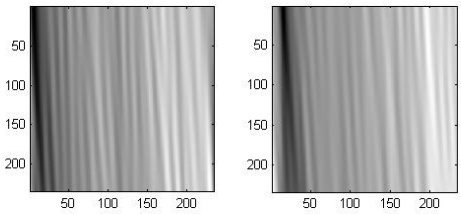

Fig.2 Radon Transform

In our experience, in order to perform the comparison of micro-striatures, we noted that the fourth wavelet decomposition level showed the most significant and the best detailed graphical response.
In the following figures it is depicted the *best matching*, found in the series of micro-striatures (Figg. 3-8).

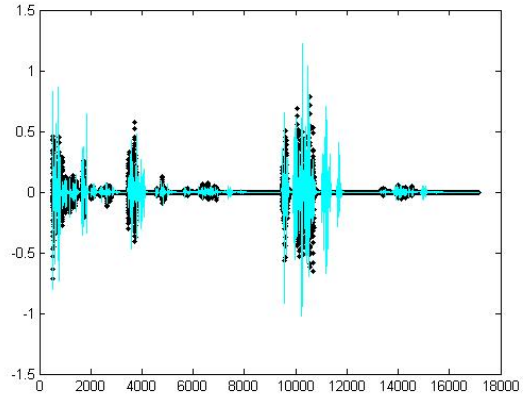

Fig. 3 Comparison of 1Aa # 2Ac

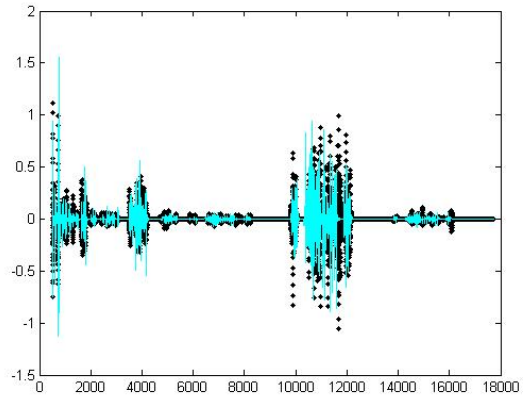

Fig. 4 Comparison of 1Ab # 2Ad

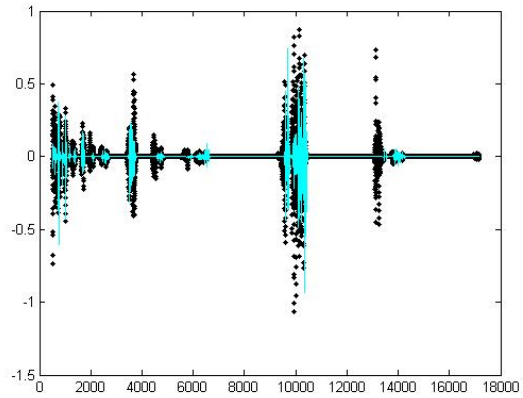

Fig. 5 Comparison of 1Ac # 2Ae

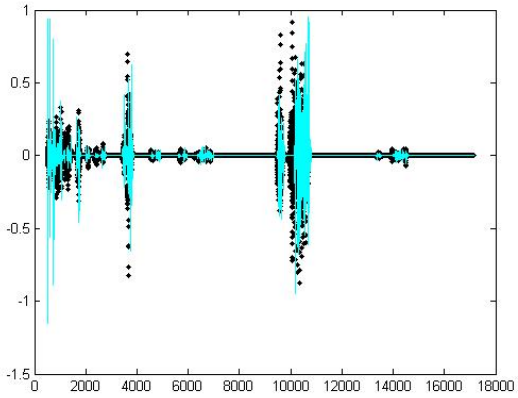

Fig. 6 Comparison of 1Ad # 2Af

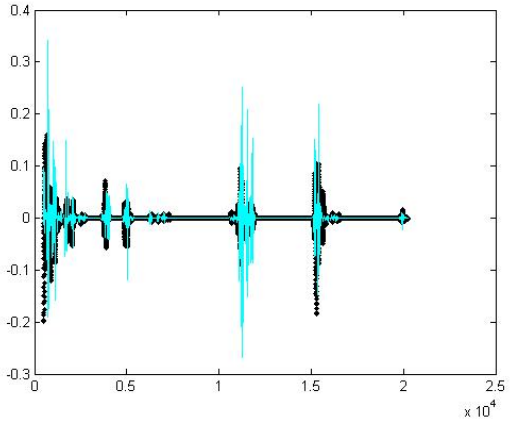

Fig. 7 Comparison of 1Ae # 2Aa

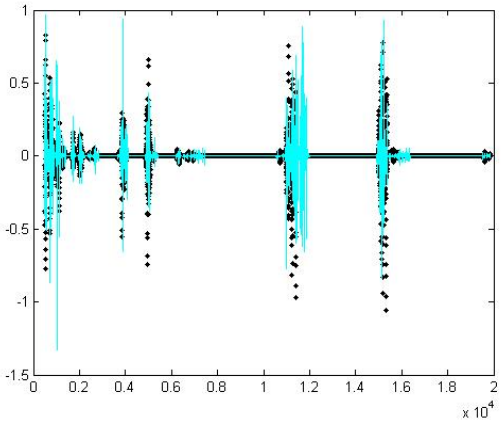

Fig. 8 Comparison of 1Af # 2Ab

In Fig.9 it is showed a random matching of two micro-striatures belonging to bullets, fired from the same gun (*i.e.*, 'A').
It is evident the *mismatch* regarding the main striatures.
In Fig.10 we can see the *best matching* between two bullets fired by two different firearms (same model) named as 'A' and 'B' respectively. As we can see, it is quite evident a significative no-overlapping-area of two series of wavelet coefficients.

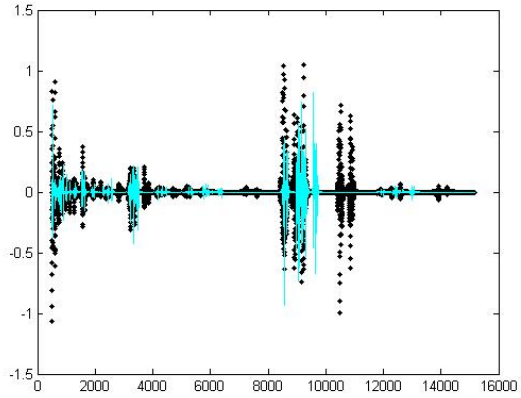

Fig.9 Micro-striatures not in the right sequence (1Aa # 2Aa).

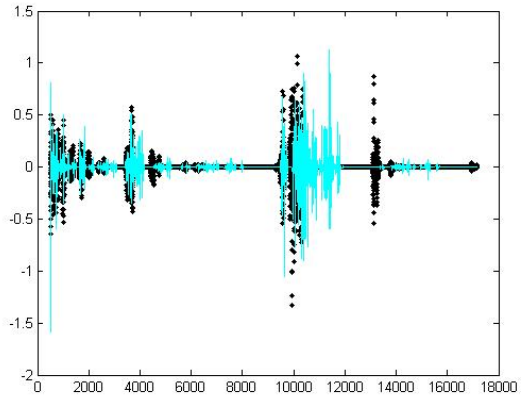

Fig.10 Comparison of two micro-striatures belonging to different guns (same model)

4 Discussion and Conclusion

In this first experience, it is important to emphasize that the order of magnitude of ROIs is roughly 1 mm^2. Considering that, commonly in ballistic forensic repertory, it is easy to handle strongly deformed bullets, this method should allow to carry over the research of firearm identification on fragments of bullet. Actually, a limit is the technique of selection of ROIs. The aim is to automize their acquisition and to improve the *best fitting* process of selected images. Currently our work is also focused on the improvement of the acquisition, in terms of resolution and lighting.
Finally, it is shown that the *RT* is able to transform each of the lines into peaks positioned corresponding to the parameters of the lines. In this way the *RT* converts difficult global detection

problem in the image domain into a more easily solved local peak detection problem in the parameter domain.
Note that especially in noisy case other algorithms in general fail. An alternative could be to use a local detection algorithm based on edge filters. Algorithms of this kind have problems with intersecting lines and in case of high noise level [21][22].
Finally, in order to improve the reliability of the proposed method, investigation will be conducted further on a wider data-base.

References:

[1] Nichols R. G., Firearm and Tool mark Identification Criteria: a Review of Literature, Part I. *J. For. Sci.*, Vol. 42, No. 3, 1997.
[2] Nichols R. G., Firearm and Tool mark Identification Criteria: a Review of Literature, Part I. *J. For. Sci.*, Vol. 48, No. 2, 2003.
[3] Ugolini A., *L'Esperto Balistico Vol.2,* Ed. Olimpia, 1984.
[4] Ugolini A., I criteri di stima statistica nella elaborazione elettronica dei parametri di identificazione dei reperti balistici a fine di prova giudiziaria, *Atti del Convegno Nazionale di Medicina Legale Lanciano 1986*, 21-22 Marzo 1986.
[5] Biasotti A., A statistical study of the individual characteristics in signatures of fired bullets, *J. For. Sci.*, Vol.4, No.1, 1959, pp. 34-50.
[6] Biasotti A., Murdock J., Criteria for identification or state of the art of firearm and tool mark identification, *AFTE Journal*, Vol.16, No.4, 1984, pp. 16-34.
[7] Bunch S.G., Consecutive matching striation criteria: a general critique, *J. For. Sci.*, Vol.45, No.5, 2000, pp. 955-962.
[8] Romano C., Quaremba G., Buccelli C., Donnarumma A., Esposito M., Pilleri M., Nuove tecniche in balistica forense per l'identificazione dei proiettili, mediante rugosimetro a raggio laser, Med. Leg. Quad. Cam., Vol.XIV, No.2, 1992, pp. 309-349.
[9] Braga A.A., Pierce G.L, Linking crime guns: the impact of ballistics imaging technology on the productivity of the Boston Police Department's Ballistics Unit, *J. For. Sci.,* Vol.49, No.4, 2004, pp. 701-706.
[10] Hough P.V.C., A method and means for recognizing complex patterns, *US Patent,* No.3,069,654, Dec. 1962.
[11] Deans S.R, Hough Transform from the Radon Transform, *IEEE PAMI*, Vol.3, No.2, 1981, pp. 185-188.
[12] Özdogan Y., *Seismic Data Processing. Soc. of Exploration Geophysicists*, Tulsa, Oklahoma, 1987.
[13] Härdle W., Kerkyacharian G., Picard D. and Tsybakov A., *Lecture Notes in Statistics - Wavelets, Approximation, and Statistical Applications*, Springer, 1998.
[14] Ogden R.T., *Essential wavelets for statistical applications and data analysis*, Birkhäuser, 1997.
[15] Daubechies I., Orthonormal bases of compactly supported wavelets, *Comms. Pure Appl. Math.*, Vol.41, No.3-4, 1988, pp. 909-996.
[16] Mallat S.G., Multiresolution approximations and wavelet orthonormal bases of L2, *Trans. Amer. Math. Soc.*, Vol.1, No.315, 1989, pp. 69-87.
[17] Meyer Y., *Wavelets and operators*, Cambridge University Press, 1990.
[18] Daubechies I., *Ten lectures on wavelets*, SIAM, 1992.
[19] Kaiser G., *A Friendly Guide to Wavelets*, Birkhäuser, 1999.
[20] Toft P., Radontrasnforrmation. *Lecture Note for DTU course 4235: Advanced Digital Signal Processing, Electronics Institute University of Denmark*, 1994.
[21] Deriche R., Using Canny's Criteria to derive a recursively implemented optimal edge detector, *Int. J. of Computer Vision*, Vol.2, No.1, 1987, pp. 167-187.
[22] Canny J., A computational approach to edge detection, *IEEE Trans. PAMI*, Vol.8, No.6, 1986, pp. 679-698.